International Journal of Railway Research, Vol. 13, No. 1, (2026), 27-36

Iran University of Science and Technology

International Journal of

Railway Research

ISSN: 2423-3838

Temperature distribution in wheel-rail contact considering roughness

Mahshad Ataei [1], Habibollah Molatefi [2*]

[1] Department of Railway Rolling Stock Engineering, School of Railway Engineering, Iran University of Science and Technology, Tehran, Tehran, Iran. mahshad_ataei@rail.iust.ac.ir

[2] Department of Railway Rolling Stocks Engineering, School of Railway Engineering, Iran University of Science and Technology, Tehran, Tehran, Iran.

ARTICLE INFO

Article history:

Received: 27.11.2025

Accepted: 18.03.2026

Published: 19.03.2026

Keywords:

Wheel-rail contact,

Coupled thermal-mechanical analysis,

Roughness,

Elastic and elastoplastic contact,

Frictional heat.

A B S T R A C T

In this paper, a multi-scale plane strain model has been developed to investigate the temperature distribution in elastic contact and then elastoplastic contact of wheel and rail considering smooth and rough surfaces for the first time. The finite element results in smooth area of elastoplastic contact indicate that due to plastic deformations, a portion of the generated energy is expended on these deformations. Consequently, the maximum temperature in this type of contact, considering that no heat is induced by plastic deformation, tends to fall around 8 % relative to elastic contact. However, a counter behavior is observed in the rough area of elastoplastic contact where the local heat in the contact area is higher and hence the temperature on the surface of asperities is higher compared to elastic contact. This may be due to the stress concentration and improper distribution of heat in the rough elastoplastic contact.

1. Introduction

The thermomechanical conditions at the wheel-rail contact are important in predicting the temperatures generated by frictional heating, which are influenced by slip, load, material properties, and surface conditions. Kapoor considered that a temperature rise would worsen wear due to plastic ratcheting [1]. It promotes the plastic flow of the surface material [2] and alters its properties and friction behavior [3]. It also contributes to martensite formation [4], thermal fatigue [5], and crack initiation and propagation [6] [7]. All these aids in the formation of defects such as hot spots, shelling, spalling, and corrugation [8]. Research [9] provided experimental validation using a twin-disc rig and thermal imaging, comparing measured temperatures against analytical models that equated frictional heat generation with conduction, convection, and radiation losses. Analytical methods, such as those developed by Knothe and Liebelt [10] and advanced by Ertz and Knothe [11], provide efficient calculations for these temperatures under Hertzian contact conditions. Subsequent study extended the analysis to the resulting thermal stresses, demonstrating their significant effect on reducing the elastic limit and shakedown limit of the material, particularly in the rail under driving conditions [12]. To overcome the simplifications of analytical approaches, Naeimi et al. [13] employed a 3D finite element model that couples mechanical and thermal solutions for a more realistic analysis of rolling contact with partial slip. To handle complex geometries and environmental factors, Vo et al. [14] employed a 3D FE model

*Corresponding author
Email address: molatefi@iust.ac.ir

of a full wheel and rail to analyze stress states, and then a theoretical thermal calculation to predict temperature variation under dry, wet, and oily contact conditions. For further refining the temperature predictions, Kennedy and Tian [15] developed comprehensive analytical models that specifically incorporated the effects of surface roughness and convective cooling to partitioned heat and calculate both nominal and flash temperature rises. At the micro-scale, a contact intensity factor is introduced to model the pressure intensification at asperities and a heat partition factor is derived that accounts for simultaneous heating from both friction and plastic deformation [16]. There is a good review of the effects of thermal load on the wheel-rail contact in [8].

In this research, the multiscale model in [17] is developed to study the temperature distribution in the wheel-rail contact area, taking into account the roughness effect by FE method for the first time. It is assumed that almost all the energy dissipated in the frictional contact is converted into heat at the actual contact surface. This frictional heat causes an increase in the temperature of the wheel-rail contact, especially near the contact surface. The increased temperature has many effects on the contact behavior. The generated heat and temperature distribution in contact area can be strongly affected by the contact pressure.

2. Materials and Methods

2.1. FEM Method

A coupled and transient thermomechanical analysis is performed, in which the heat dissipated due to friction is completely converted into heat in the contact area. In this study, the rough finite element model described in [17] is developed. The rough area is modeled as a sine-generated curve with an average radius of 1.25 mm and a length of 1 mm along the rail surface. The wavelength and amplitude of the asperities are 200 and 2 microns, respectively. Consequently, the rough area contains a total of five asperities. The remainder of the rail surface is smooth. The entire wheel surface is characterized by smoothness. This multi-scale model is illustrated in Figure 1.

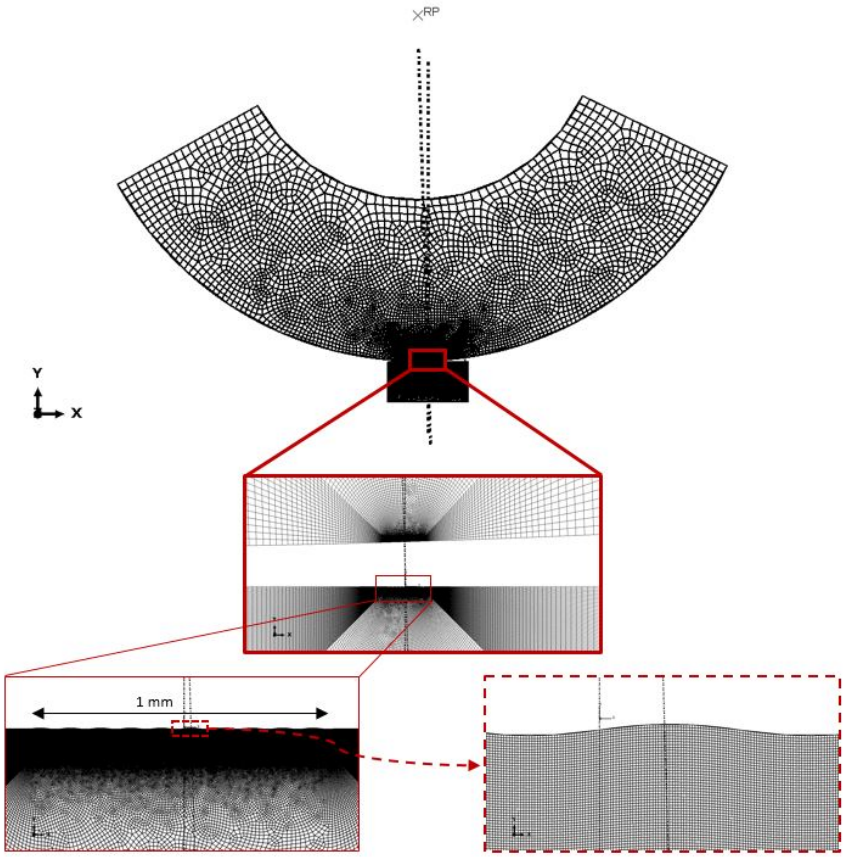

Figure 1 - Two-dimensional multiscale plane-strain model with surface roughness [17]

In the small area of the wheel and rail, the element length is 5 microns going to surface of the wheel and rail, the element size is smaller and equal to 1 micron. For both wheel and rail, linear plane strain elements coupled with temperature (CPE4T) are considered. The number of rail elements in the small rough area is 100,000, and the number of wheel elements in the small smooth area is 6,660. The total elements in the other areas of the rail are 77,952, and 17,548 for the wheel. In Figure 2, the wheel-rail assembly model is shown along with the loading and boundary conditions of the problem; the bottom surface of the rail has a fixed constraint in the vertical direction, and the side surfaces are fixed in the horizontal direction. All loadings are applied at the center of the wheel. The vertical force (F_N) is equal to 10 kN (approximately equivalent to the wheel force of 80 kN in the 3D case [18]). A clockwise angular displacement (1) of 0.0605 radian, a tangential horizontal force (F_T) of 3 kN in the opposite direction of movement, and an initial translational velocity of 80 km/h are also applied to the wheel center. Accordingly, the traction coefficient (T) between the wheel and the rail is determined to be 0.3 (2). The wheel moves quasi-statically on the rail, without any dynamic effects. The initial temperature of the wheel and the rail is assumed to be 25 degrees.

$$\phi_z = \frac{l_{roll}(2+c)}{R_{wheel}(2-c)} \tag{1}$$

$$T = \frac{F_T}{F_N} \tag{2}$$

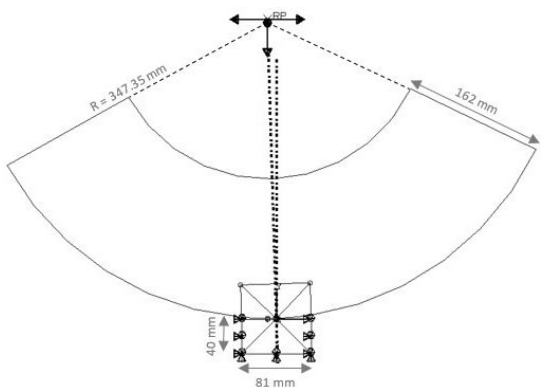

Figure 2 - Loading and boundary conditions of the problem

The mechanical and thermal properties of the wheel and rail are evaluated in accordance with Table 1. The plastic behavior of the rail follows the Chaboche kinematic hardening law in which the values of the back-stress parameters (Ci and γ_i) are given in Table 2. Given the uniform thermal properties of the wheel and rail, the heat partitioning factor (ε) depends only and slightly on the wheel speed according to the size of the contact area. Therefore, for the sake of simplicity, it is assumed that the heat partition factor to the wheel and rail is the same and equal to 0.5 [7] [12]. Heat due to plastic deformation, convection and radiation are neglected.

Table 1 - Thermomechanical properties of wheels and rails

Parameter	Wheel	Rail
Mechanical Properties		
Young's modulus (GPa)	210	206
Poisson's ratio	0.3	0.28
Initial yield stress (GPa)	-	320
Thermal properties		
Conductivity (W/m°C)	45	45
Thermal Expansion (1/°C)	1.1×10^{-5}	1.1×10^{-5}
Specific heat capacity (J/kg°C)	500	500
Density (kg/m^3)	7800	7800

Table 2- Six back-stresses of the rail

i	C_i (GPa)	γ_i
1	350	5000
2	80	1000
3	15	150
4	10	50
5	8	20
6	0.19	0.01

Normal contact is defined as hard contact. The relationship between contact pressure and overclosure is linear and the overclosure value at the beginning of contact is assumed to be 0.01. The wheel travels a total distance of 21 mm from 10 mm before the rough area to 10 mm after the rough area. The friction coefficient is assumed to

be 0.5. The elastic slip value is 0.0001. The slip rate created between the wheel and the rail is obtained from the following equation:

$$c = \frac{2(V_t - V_r)}{V_t + V_r} \quad , \quad V_{t,r} > 0 \tag{3}$$

2.2. Analytical Method

When the wheel and rail are in contact under the wheel static force, the contact area and pressure distribution are evaluated by Hertz's theory. In a two-dimensional plane strain contact under a vertical force per unit length N/b^*, the normal pressure distribution is as follows [19]:

$$p_z(x) = p_0\sqrt{1 - \frac{x^2}{a^2}} \tag{4}$$

Where the maximum hertzian pressure is:

$$p_0 = \frac{2N}{\pi a b^*} \quad , \quad b^* = \frac{4}{3}b \tag{5}$$

By comparing the maximum pressure in the two-dimensional case with the three-dimensional case, the length parameter b^* is defined as the basis for transferring the problem from the 3D to the 2D problem.

The presence of tangential force creates a speed difference between the wheel and the rail, resulting in an average relative velocity at the contact point (Figure 3). If the value of this relative velocity is high, the temperature of the contact area will be high, too [11].

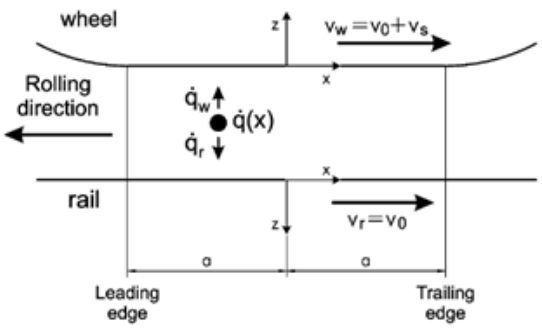

Figure 3 - Distribution of frictional heat generated in the wheel-rail contact area [11]

In the very short time that the surface points are in contact with each other, the thermal penetration depth (δ) is very small compared to the size of the contact area and can be calculated as follows:

$$\delta = \frac{a}{\sqrt{L}} \tag{6}$$

Where L is the dimensionless Peclet number. L can be defined as the ratio of the contact surface velocity to the rate of heat diffusion into the material, as below:

$$L = \frac{av}{2\kappa} \quad , \quad \kappa = \frac{k}{\rho C} \tag{7}$$

a is the half-length of the contact patch, v is the linear velocity of the moving heat source (here the wheel speed), κ is the thermal diffusivity, k is the thermal conductivity coefficient, ρ is the density and C is the specific heat capacity. Since the wheel and rail speeds in the contact area are different, this must be taken into account in calculating the Peclet number and the heat penetration depth. If $L > 10$, the heat conduction is perpendicular to the contact plane [11] (Figure 3). The conduction heat transfer equation is as follows:

$$\kappa \frac{\partial^2 \Theta}{\partial z^2} = \frac{\partial \Theta}{\partial t} \tag{8}$$

The initial temperature is room temperature and Θ represents the temperature rise. With constant values of the friction coefficient and sliding velocity (v_s), the rate of frictional energy dissipation in the contact area is proportional to the contact pressure and is equal to [11]:

$$q_{friction}(\xi) = \mu v_s p_z(\xi) = \mu v_s p_0 f(\xi) \tag{9}$$

Assuming that all frictional energy is converted to heat, the frictional heat distribution in Hertzian contact is equal to [12]:

$$q_{friction}(\xi) = \mu v_s p_0 \sqrt{1 - \xi^2} \tag{10}$$

If we assume that all the heat generated by friction is transferred to the wheel and rail, part of this heat is transferred into the wheel (q_w) and another part into the rail (q_r), as below:

$$q_w(\xi) = \varepsilon q_{friction}(\xi) \tag{11}$$

Table 3 - A comparison of the maximum contact surface temperature gradient between finite element and analytical solutions in elastic wheel-rail contact

Max. contact temperature rise in [11]	Simple estimation*	Improved approximation**
	$\theta_{max} = 1.253 \frac{\varepsilon \mu v_s p_0}{\beta_r} \sqrt{\frac{a}{v_r}}$	$\theta_{max}(\xi) = \frac{\varepsilon \mu v_s p_0}{\beta_r} \sqrt{\frac{a}{\pi v_r}} F(\xi)$
	30.02°C	27.71°C
FEM solution	28.53 °C	
Deviation	4.96%	2.96%

* at the trailing edge

** $F(\xi) = \frac{\pi}{128}\sqrt{\xi+1}(71+12\xi-20\xi^2+8\xi^3-16\xi^4)$, $-1 \le \xi \le 1$

$\xi = \frac{x}{a}$, $\zeta = \frac{z}{\delta}$

$$q_r(\xi) = (1-\varepsilon) q_{friction}(\xi) \tag{12}$$

A number of methodologies have been developed to calculate the temperature rise and temperature distribution in the contact area. Among these, the analytical solutions of Ertz [12] [11] are used in this study, wherein elastic material and the Hertzian pressure are taken into account. The thermal penetration coefficient β_r of the rail is as follows:

$$\beta_r = \sqrt{k_r \rho_r C_r} = \frac{k_r}{\sqrt{\kappa_r}} \tag{13}$$

A simple estimation and an improved approximation for the calculation of the maximum temperature rise in the wheel-rail contact area are given in Table 3. The sliding velocity in these relations is replaced by the product of the creepage and the translational velocity.

2.3. Assumptions

In order to find the temperature distribution in the contact area, first the mesh sensitivity analysis is done for the average temperature in the smooth and rough areas in elastic contact (please see Table 4). Wheel and rail have the same thermomechanical properties. Similar to

Table 4 - Mesh sensitivity analysis for coupled thermal-mechanical analysis

Case No.		Element Size (mm)		Mean temperature in smooth region (°C)	Mean temperature in rough region (°C)
		Small Region	Big Region		
0	Rail	0.01	0.01-3	25.4	26.21
	Wheel		0.01-8		
1	Rail	0.005	0.005-3	26.01	27.49
	Wheel		0.005-8		
2	Rail	0.004-0.005	0.004-2	25.23	25.01
	Wheel		0.004-8		
3	Rail	0.003-0.005	0.003-2	25.66	26.43
	Wheel		0.005-8		
4	Rail	0.002-0.005	0.002-2	25.27	25.07
	Wheel	as Case No 3	as Case No 3		
5	Rail	0.0016-0.005	0.0016-2	25.74	26.43
	Wheel	as Case No 3	as Case No 3		
6	Rail	0.0013-0.005	0.0013-2	26.7	26.89
	Wheel	as Case No 3	as Case No 3		
7	Rail	0.0011-0.005	0.0011-2	26.72	26.88
	Wheel	as Case No 3	as Case No 3		
8	Rail	0.001-0.005	0.001-2	26.73	26.88
	Wheel	as Case No 3	as Case No 3		

the analysis performed in [17], the element size of the last meshing pattern is used for subsequent analysis.

In the next step, the validity of the finite element results with those of the analytical solutions is investigated in elastic contact. Here, the elastic material of the wheel and rail is considered to be identical and consistent with the elastic properties of the wheel as shown in Table 1. Finally, the temperature distribution of elastoplastic contact is inspected in this paper.

Other assumptions that we made through the simulations are as follows:

- ✓ Transient thermal analysis
- ✓ $\varepsilon = 0.5$
- ✓ No convection or radiation
- ✓ No plastic deformation heat
- ✓ Frictional heat
- ✓ Initial temperature 25°C
- ✓ Perpendicular heat transfer
- ✓ Translational velocity 80 km/h
- ✓ $\mu = 0.5$
- ✓ Global (nominal) creepage is 0.00457

3. Results & Discussion

Heat is generated due to friction between the surfaces of the wheel and rail during the rolling-sliding contact, thereby leading to an increase in the contact temperature. Moreover, given that the maximum temperature occurs at the end of the rolling distance and on the surface of the contact area, the maximum temperature in the smooth area is reported subsequent to the rough area.

3.1. Temperature distribution in elastic contact

Considering $L \approx 6316$ in our study, it can be concluded that the heat transfer is perpendicular to the contact area and the longitudinal and transverse heat transfer are ignored. Furthermore, given that the contact area is 13.12 mm in this analysis, the estimated depth of heat penetration is approximately 0.08 mm.

In the finite element model of elastic wheel-rail contact, the maximum temperature in the smooth area is 53.53 °C, located after the rough region. Please see Figure 4 (top). Consequently, the maximum temperature increase is 28.53°C, which has an error percentage of 4.96% relative to the simple estimation solution and of 2.96%

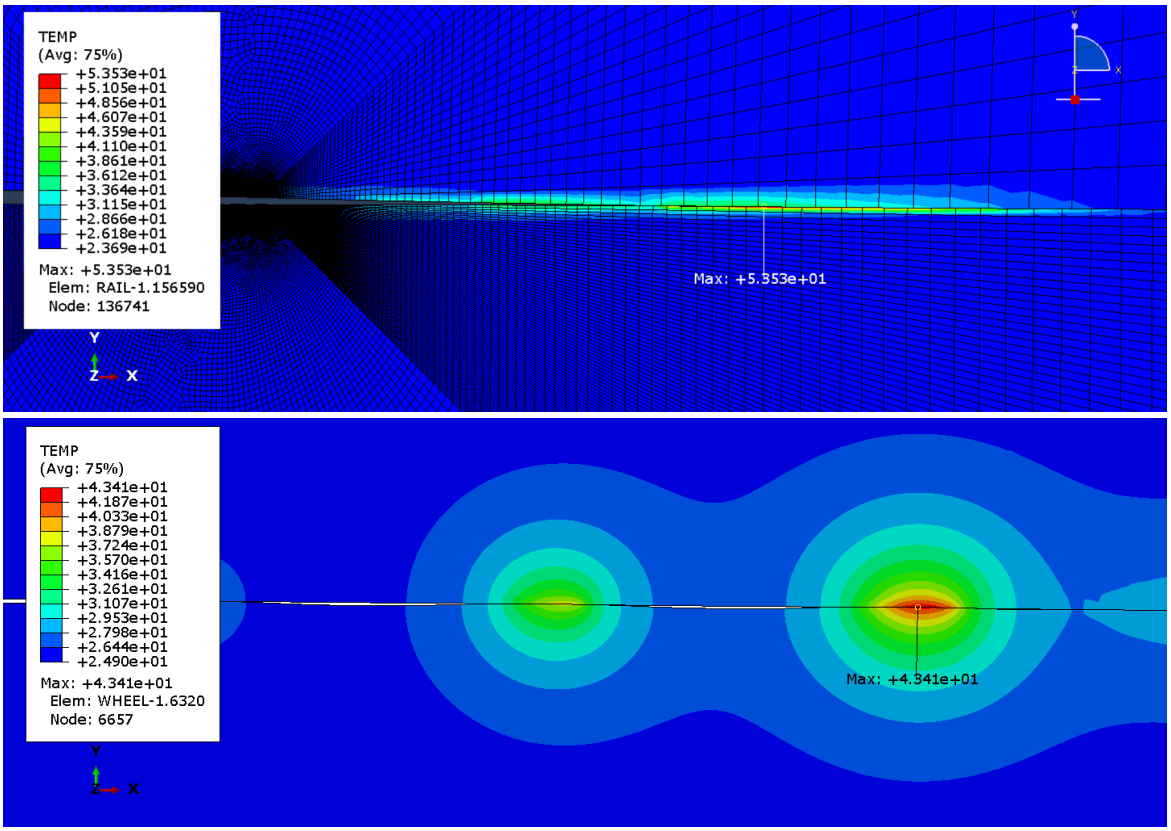

Figure 4 – Maximum temperature in elastic contact (top) smooth region (bottom) rough region

relative to the improved approximation solution (Table 3). According to the percentage of errors obtained and in accordance with the recognition of reference [11], the improved Ertz analytical solution is the most suitable closed-form analytical solution for determining the temperature of the Hertz contact area. In the small contact area between wheel and rough rail, the maximum temperature recorded with about 10 % drop to 43.41 °C on the wheel surface. Please see Figure 4 (bottom).

Figure 5 shows the distribution of contact pressure and shear stress in rough and smooth regions for a node with the maximum temperature. The level of normal and tangential stresses on the wheel surface in the rough region is approximately twice that in the smooth rail region.

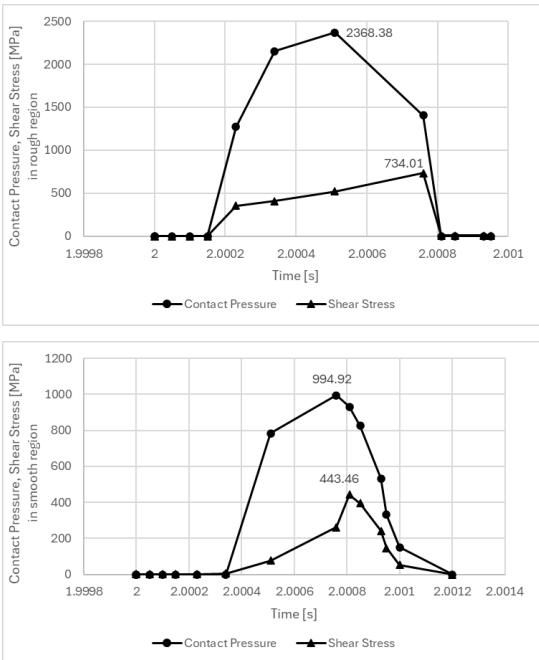

Figure 5 – Contact pressure and shear stress distribution at a node with maximum temperature on the contact surface of (top) rough region and (bottom) smooth region

3.2. Temperature distribution in elastoplastic contact

To obtain the temperature distribution in elastoplastic contact, the rail material is considered to be elastoplastic (see Table 1 and Table 2). The maximum temperature in the smooth region is 45.66 °C. The number increases up to 50.03 °C at the small contact area on the wheel.

By comparing the maximum temperatures in elastic and elastoplastic contact (Figure 6), as we expected, the maximum temperature in the smooth elastic contact tends to rise than in elastoplastic contact because the energy due to friction is mainly dissipated as heat and the material completely returns to its original state in elastic rail. However, in smooth elastoplastic contact a part of the energy is stored as plastic deformation in the rail, resulting in a reduction in the amount of heat produced. Additionally, due to the greater hardness of the contact surface in an elastic contact, the stress level is higher, leading to more heat generation in the contact area. Consequently, the temperature in smooth region exceeds that of the elastoplastic contact. These objectives are realized in the smooth region.

The results in the rough area, however, exhibit a different pattern (please see Figure *6*). In the context of an elastoplastic rail with roughness, the contact points within the peaks undergo plastic deformation. While a portion of the energy generated at the contact surface is allocated to permanent deformation, due to plastic behavior, the damaged contact points can lead to increased friction and stress concentration and consequently, more local heat in the rough area. Furthermore, plastic behavior can cause the heat generated in the small rough area to not be well distributed, resulting in an elevated surface temperature of the contact, here wheel surface.

4. Conclusions

A multiscale plane strain model of a wheel and a rough rail is utilized to analyze the thermomechanical coupling of elastic and elastoplastic contact. The results are compared with the results of closed-form analytical solutions Considering the low error rate, the FE method has very good accuracy in elastic contact. Subsequently, this method is applied to the elastoplastic wheel-rail contact. The findings demonstrate that the temperature of the smooth area in elastic contact is 53.53 °C by a rise of approximately 8 % relative to elastoplastic contact. This is due to the fact that, a portion of the generated energy is allocated to plastic deformation, resulting in a reduction in the

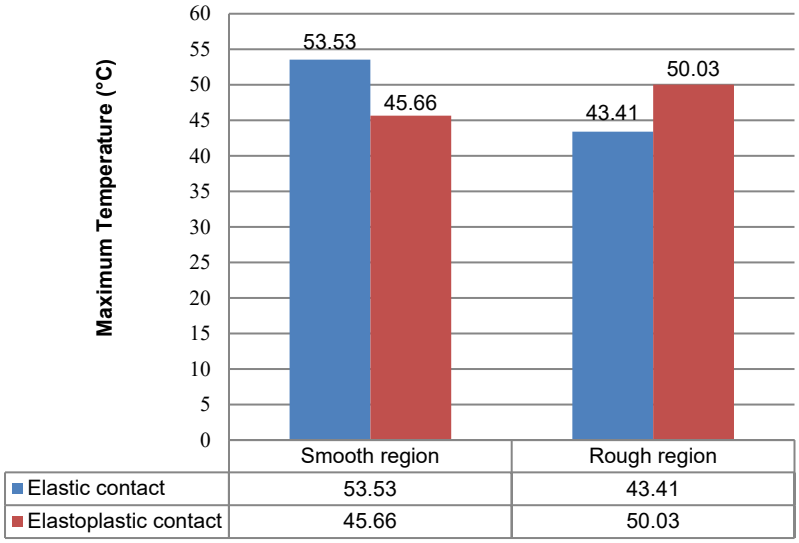

Figure 6- Maximum temperature in the smooth and rough regions of elastic and elastoplastic contact problems

amount of heat generated during elastoplastic contact. However, an alternate vice versa behavior is observed in the rough area. The plastic deformation of the damaged contact points has been shown to result in increased friction and stress concentration. This, in turn, leads to the observation of greater local heat and an elevated surface temperature of the asperities in comparison to that of elastic contact.

Declaration of Conflicting Interests

The authors declared no potential conflicts of interest with respect to the research, authorship, and/or publication of this article.

Acknowledgements

The authors appreciate Fast Computing Center and Technical Documentation Center of the Iran University of Science and Technology for providing the facilities needed for this work.

List of symbols

English symbols

a	Half-length of contact patch
b	Half-width of contact patch
b^*	Length parameter
c	Creepage (Slip rate)
C	Specific heat capacity
C_i	Back-stress parameter
C_r	Back-stress parameter of rail
F_N	Vertical force
F_T	Tangential horizontal force
k	Thermal conductivity coefficient
k_r	Thermal conductivity coefficient of rail
l_{roll}	Rolling distance
L	Peclet number
N	Normal load
p_z	Pressure distribution
p_0	Maximum Hertzian pressure
$q_{friction}$	Rate of frictional energy dissipation
q_w	Wheel frictional energy dissipation rate
q_r	Rail frictional energy dissipation rate
R_{wheel}	Wheel radius
t	time
T	Traction coefficient
v	Linear velocity
v_r	Rail velocity
v_s	Sliding velocity
V_r	Rotational velocity
V_t	Translational velocity
x	Longitudinal location
z	Vertical location

Greek symbols

β	Thermal penetration coefficient
β_r	Thermal penetration coefficient of rail
δ	Penetration depth
ε	Heat partitioning factor
ϕ_z	Angular displacement
γ_i	Back-stress parameter

κ	Thermal diffusivity
κ_r	Thermal diffusivity of rail
μ	Friction coefficient
θ_{max}	Maximum contact temperature rise
Θ	Temperature rise
ρ	Density
ρ_r	Density of rail
ξ	Non-dimensional longitudinal location
ζ	Non-dimensional vertical location

References

[1] A. Kapoor, "Wear by plastic ratchetting," Wear, vol. 212, no. 1, pp. 119-130, 1997.

[2] T. Vernersson, S. Caprioli, E. Kabo, H. Hansson and A. Ekberg, "Wheel tread damage: A numerical study of railway wheel tread plasticity under thermomechanical loading," Proceedings of the Institution of Mechanical Engineers, Part F: Journal of Rail and Rapid Transit, vol. 224, no. 5, pp. 435-443, 2010.

[3] D. Thuresson, "Influence of material properties on sliding contact braking applications," Wear, vol. 257, no. 5-6, pp. 451-460, 2004.

[4] J. Jergéus, "Martensite formation and residual stresses around railway wheel flats," Proceedings of the Institution of Mechanical Engineers, Part C: Journal of Mechanical Engineering Science, vol. 212, pp. 69-79, 1998.

[5] A. Ekberg and E. Kabo, "Fatigue of railway wheels and rails under rolling contact and thermal loading - an overview," Wear, vol. 258, no. 7-8, pp. 1288-1300, 2005.

[6] S. Caprioli, T. Vernersson and A. Ekberg, "Thermal cracking of a railway wheel tread due to tread braking–critical crack sizes and in fluence of repeated thermal cycles," Proceedings of the Institution of Mechanical Engineers, Part F: Journal of Rail and Rapid Transit, vol. 227, no. 1, pp. 10-18, 2012.

[7] A. Haidari and P. Hosseini Tehrani, "Thermal load effects on fatigue life of a cracked railway wheel," Latin American Journal of Solids and Structures, vol. 12, pp. 1144-1157, 2015.

[8] J. P. Srivastava, P. K. Sarkar and V. Ranjan, "Effects of thermal load on wheel–rail contacts: A review," Journal of Thermal Stresses, vol. 39, no. 11, pp. 1389-1418, 2016.

[9] E. A. Gallardo-Hernandez, R. Lewis and R. S. Dwyer-Joyce, "Temperature in a twin-disc wheel/rail contact simulation," Tribology International, vol. 39, pp. 1653-1663, 2006.

[10] K. Knothe and S. Liebelt, "Determination of temperatures for sliding contact with applications for wheel-rail systems," Wear, vol. 189, pp. 91-99, 1995.

[11] M. Ertz and K. Knothe, "A comparison of analytical and numerical methods for the calculation of temperatures in wheel/rail contact," Wear, vol. 253, pp. 498-508, 2002.

[12] M. Ertz and K. Knothe, "Thermal stresses and shakedown in wheel/rail contact," Archive of Applied Mechanics, vol. 72, pp. 715-729, 2003.

[13] M. Naeimi, Z. Li, R. Dollevoet, J. Wu, R. H. Petrov and J. Sietsma, "Computation of the flash-temperature at the wheel-rail contact using a 3D finite element model and its comparison with analytical methods," in 10th International Conference on Contact Mechanics, Colorado Springs, 2015.

[14] K. D. Vo, A. K. Tieu, H. T. Zhu and P. B. Kosasih, "A tool to estimate the wheel/rail contact and temperature rising under dry, wet and oily conditions," Computers in Railways XIV, vol. 135, pp. 191-201, 2014.

[15] F. E. Kennedy and X. Tian, "Modeling sliding contact temperatures, including effects of surface roughness and convection," Journal of Tribology, vol. 138, no. 4, 2016.

[16] F. D. Fischer, W. Daves and W. E. A, "On the temperature in the wheel-rail rolling contact," Fatigue & Fracture of Engineering Materials & Structures, vol. 26, no. 10, pp. 999-1006, 2003.

[17] M. Ataei and H. Molatefi, "Influence of friction and dynamic wheel load coefficients on wheel-rail contact considering different roughness dimensions," Proceedings of the Institution of Mechanical Engineers, Part J: Journal of Engineering Tribology, vol. 0, no. 0, pp. 1-15, 2025.

[18] W. Daves, W. Kubin, S. Scheriau and M. Pletz, "A Finite Element Model to Simulate the Physical Mechanisms of Wear and Crack Initiation in Wheel/Rail Contact," Wear, Vols. 366-367, pp. 78-83, 2016.

[19] J. K. L, Contact mechanics, Cambridge: Cambridge University Press, 1985.